Volume 49
Number 42
14 November 2025
Pages 18205–18668

NJC

New Journal of Chemistry

A journal for new directions in chemistry

rsc.li/njc

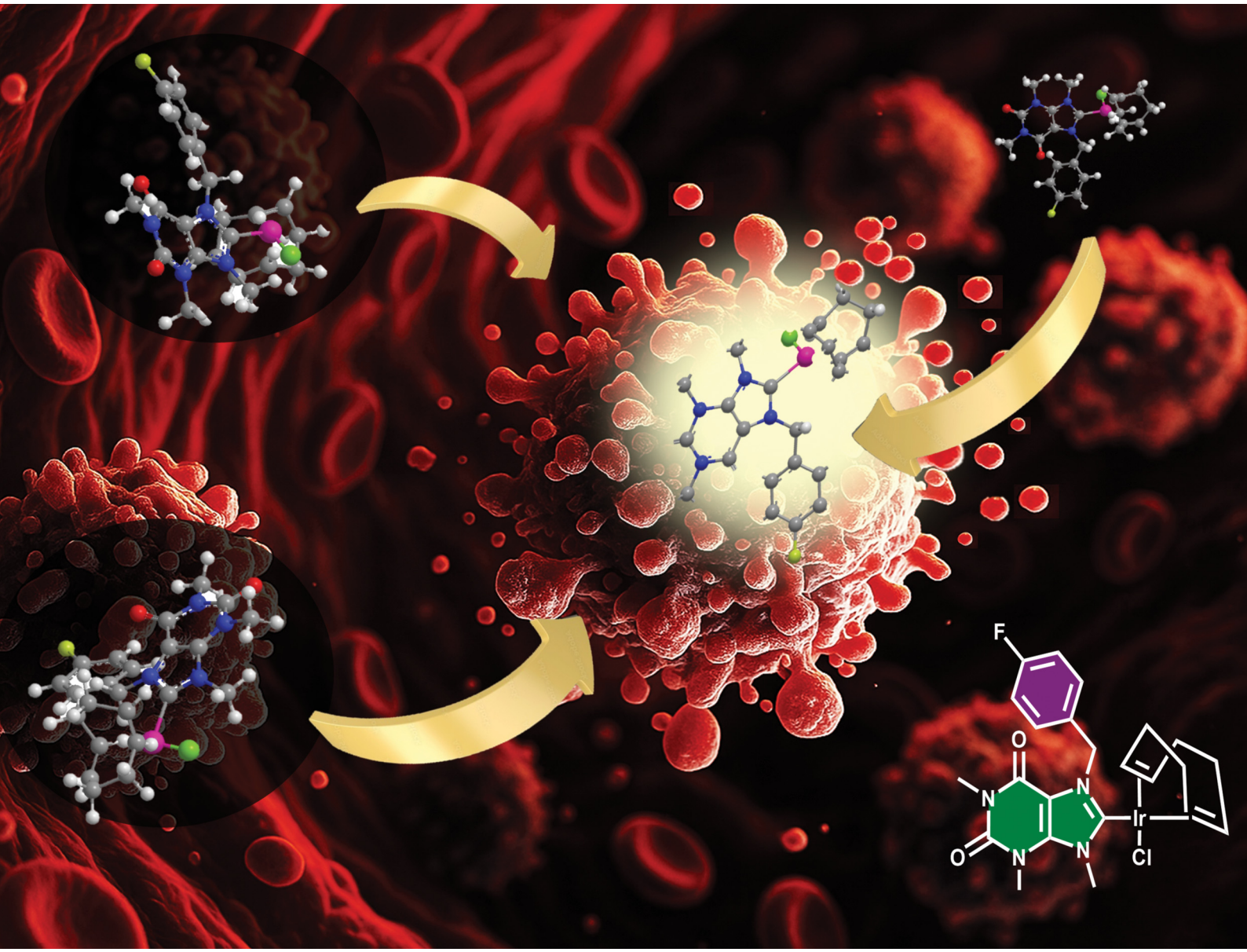

ISSN 1144-0546

ROYAL SOCIETY OF CHEMISTRY

PAPER

David Morales-Morales *et al.*

Theophylline-based NHC–Ir(I) complexes bearing fluorinated benzyl groups as potential anticancer agents

cnrs

NJC

ROYAL SOCIETY OF CHEMISTRY

PAPER

View Article Online
View Journal | View Issue

Cite this: *New J. Chem.*, 2025, **49**, 18258

Theophylline-based NHC–Ir(I) complexes bearing fluorinated benzyl groups as potential anticancer agents†

Arturo Sánchez-Mora,[a] Lucero González-Sebastián,[b] J. Antonio Cruz-Navarro,[a] Antonino Arenaza-Corona,[a] Teresa Ramírez-Apan,[a] Antonio Nieto-Camacho[a] and David Morales-Morales *[a]

In this study, we present the synthesis, comprehensive characterization, and biological evaluation of a novel series of N-heterocyclic carbene iridium(I) (NHC–Ir(I)) complexes derived from theophylline. The structures of both the theophylline-based ligands and their corresponding metal complexes were elucidated using a combination of spectroscopic techniques, including multinuclear NMR, ATR-FTIR spectroscopy, mass spectrometry, and elemental analysis. We investigated the impact of fluorine substitution on the theophylline core, as well as the role of auxiliary ligands—cyclooctadiene (COD, complexes **3a–e**) and carbonyl (CO, complexes **4a–e**) on the coordination environment of the Ir(I) center. The cytotoxic activity of the synthesized complexes was evaluated against six human cancer cell lines, revealing insights into structure–activity relationships. While the free ligands exhibited no cytotoxicity, their NHC–Ir(I) complexes significantly enhanced anticancer activity. Among the tested complexes, those containing COD ligands (**3a–e**) demonstrated the highest cytotoxic potency. This effect was attributed to the challenges in oxidizing Ir(I) to its active Ir(III) species when CO ligands were present. Antioxidant assays and preliminary electrochemical studies confirmed that the formation of Ir(III) species play a crucial role in the observed cytotoxicity. Among all the complexes, **3c** exhibited the most promising profile, showing potent activity against K-562, PC-3, and SKLU-1 cancer cells, with IC_{50} values of 5.4 ± 0.2, 5.7 ± 1.0, and 8.5 ± 0.7 μM, respectively. Furthermore, complex **3c** showed minimal toxicity toward healthy COS-7 cells and exhibited favorable physicochemical properties (log *D* = 2.87).

Received 1st June 2025,
Accepted 15th July 2025

DOI: 10.1039/d5nj02288f

rsc.li/njc

1. Introduction

The use of organometallic and coordination complexes in anticancer drug design has attracted considerable attention in recent years due to the significant challenges cancer poses to global health. In 2022, the International Agency for Research on Cancer (IARC) reported 20 million new cases and 9.7 million cancer-related deaths worldwide.[1] While chemotherapy remains the primary treatment approach, the structural versatility of metallodrugs provides a unique opportunity for developing innovative anticancer therapies. In general, metallodrugs offer a diverse range of compounds with varied mechanisms of action, often overcoming the limitations of purely organic drugs by allowing modifications of ligands, metal centers, and oxidation states.[2–5] Since the FDA approval of cisplatin in 1978, a wide variety of metallodrugs incorporating metals such as gold (Au), copper (Cu), vanadium (V),[6] ruthenium (Ru), nickel (Ni)[7,8] and zinc (Zn),[9] have been investigated to address challenges such as chemoresistance[10] and the toxicity[11,12] associated with platinum-based therapies.

N-heterocyclic carbene (NHC) ligands have emerged as important components in metallodrug development due to their strong σ-donating ability, ease of synthesis, and capacity to form stable bonds with a wide range of transition metals. These highly tunable ligands, modifiable through substituent alterations on nitrogen atoms, play a crucial role in determining the stability, solubility, and lipophilicity of metal complexes. Over the past two decades, NHC ligands have gained significant attention in medicinal chemistry, particularly in the design of anticancer and antimicrobial agents.[10–12] Notably, NHCs can be synthesized from xanthines, a versatile class of compounds that includes well-known examples such as caffeine, theophylline, and theobromine. The intrinsic biological

[a] *Instituto de Química, Universidad Nacional Autónoma de México, Circuito Exterior, Ciudad Universitaria, Ciudad de México, C.P. 04510, Mexico. E-mail: damor@unam.mx*
[b] *Departamento de Química, Universidad Autónoma Metropolitana-Iztapalapa, Av. San Rafael Atlixco No. 186, Ciudad de México, C.P. 09340, Mexico*

† Electronic supplementary information (ESI) available. See DOI: https://doi.org/10.1039/d5nj02288f

activity of xanthines, combined synergistically with the properties of the metal center, underscores their potential as exceptional candidates for the development of innovative metallodrugs.[13,14] For instance, Willans and coworkers reported a series of Ag-NHCs derived from theophylline that exhibited moderate activity against HCT116 and Panc-1 (colon and pancreatic adenocarcinoma) cell lines, with IC_{50} values of approximately 20 μM.[15] Similarly, Visentin described palladium-based NHC complexes with significantly higher cytotoxic activity, reaching the nanomolar scale against A2780 (ovarian carcinoma).[16]

Iridium(I) complexes have emerged as promising candidates in medicinal chemistry due to their structural similarities to platinum(II) complexes, which are well known for their anticancer properties. However, significant progress in the development of Ir(I) complexes did not occur until 2015, when Metzler-Nolte's group identified the antiproliferative properties of the **1-Ir** complex (Fig. 1) in MCF-7 and HT-29 cell lines. Their study highlighted its prodrug behavior and oxidative interaction with cytochrome *c*,[17] marking the inception of a novel class of first-in-class (FIC) drugs. This breakthrough has since inspired further research into ligand modifications to enhance their therapeutic activity.[18,19] The most recent complexes (**6-Ir** and **7-Ir**) were reported by the Karataş group, demonstrating significant anticancer activity, particularly against the ovarian cancer cell line A2780.[20,21] In this context, our research group has reported the synthesis of a series of iridium complexes containing 5,6-dinitrobenzimidazole[22] and theophylline.[23] Ligands (**4-Ir** and **5-Ir**, Fig. 1), along with their cytotoxic evaluation in various cancer cell lines. Notably, iridium complexes with theophylline ligands (when X = Cl) exhibited significant cytotoxic activity, particularly against PC-3 and SKLU-1 cancer cells, with IC_{50} values of 7.8 ± 0.4 μM and 10.7 ± 0.7 μM, respectively. Building on these promising results and the aimed to develop a more potent and selective Ir(I)-based metallodrugs, we present in this study the synthesis of a new series of Ir(I) N-heterocyclic carbene (NHC) complexes derived from theophylline substituted with fluorinated benzyl moieties *via* N-alkylation, which have been designed aiming to enhance their cytotoxic activity. This hypothesis has been postulated since it is well known that the introduction of fluorinated moieties, increases the lipophilic nature, favoring *in vivo* uptake and transport in biological systems, thereby enhancing their biological activity.[24,25] For instance, Li *et al.* conducted UV-visible binding affinity experiments using circulating tumor DNA, revealing that the DNA-binding ability of the acyl-hydrazone porphyrin Cu(II) complexes followed the trend: CuP3 (2,3,4,5,6-pentafluorophenyl) > CuP1 (4-fluorophenyl) > CuP2 (4-trifluoromethylphenyl).[26] These results highlight the important role of fluorine incorporation. However, no systematic SAR or QSAR studies have yet explored the influence of the number or position of fluorine atoms in Ir(I)–NHC complexes. Thus, this work represents an exploratory approach to evaluate such effects on cytotoxic performance. Furthermore, the effect of the COD and CO ligands in the anticancer activity was evaluated. Finally, the partition coefficient (log *D*), a property that has been relatively unexplored, was calculated for all complexes.

2. Results

2.1. Synthesis and structural characterization

The synthesis of imidazolium salts from theophylline was carried out through a two-step procedure, as outlined in Scheme 1. In the first step, theophylline was benzylated using the corresponding fluorinated benzyl halide in the presence of potassium carbonate, with acetonitrile as the solvent. This reaction yielded compounds (**1a–e**) with varying degrees of substitution in moderate yields. These compounds were characterized by multinuclear NMR spectroscopy (^1H, $^{13}C\{^1H\}$, and $^{19}F\{^1H\}$) and mass spectrometry, with full details provided in the Experimental section. In the second step, compounds **1a–e** were reacted with trimethyloxonium tetrafluoroborate in MeCN at room temperature for two days. The resulting azolium salts (**2a–e**) were purified by crystallization in hot methanol, yielding pure compounds in good to excellent yields, ranging from 88.5% to 95.4%. After isolation, precursor ligands **2a–e** were characterized by NMR spectroscopy, mass spectrometry, HPLC-PDA, and elemental analysis (see ESI†). The ^1H NMR spectra of all compounds show a key singlet corresponding to the NC**H**N proton, appearing in the range of 9.28 to 9.42 ppm. The procarbenic carbon N**C**HN was observed in the $^{13}C\{^1H\}$ NMR spectra between 139.4 and 139.9 ppm. The molecular ion *m*/*z* $[M - BF_4]^+$ for compounds **2a–c**, **2d**, and **2e** was observed at 303, 375, and 321, respectively. All these data are consistent with the proposed molecular structures for ligands **2a–e**.

With the precursor ligand in hand, the synthesis of NHC–Ir(I) complexes (**3a–e**) was carried out using Schlenk techniques *via in situ* deprotonation of the azolium salts with ^{t}BuOK in the presence of $[IrCl(COD)]_2$ in dry THF, as outlined in Scheme 1. After purification by column chromatography, complexes (**3a–e**) were isolated as yellow solids in moderate yields (45–61%). The $^{13}C\{^1H\}$ NMR spectra of all iridium complexes exhibited a characteristic signal between 188.4 and 190.6 ppm, attributed to the metalated carbon. Additionally, ^1H and ^{19}F NMR spectroscopy confirmed the proposed molecular structures. Notably, in the ^1H NMR spectrum, the singlet corresponding to the NCHN proton in the free ligands, observed in the range of 9.28 to 9.42 ppm, disappeared upon complex formation, supporting successful coordination to the metal center. The resulting HR-MS data are consistent with the formation of complexes **3a–e**, showing the molecular ions *m*/*z*: **3a**, calc. for $C_{23}H_{27}ClFIrN_4O_2$ 638.14358 $[M + H]^+$, found: 638.14547, **3b**, calc. for $C_{23}H_{27}FIrN_4O_2$ 603.17473 $[M - Cl]^+$, found 603.17643, **3c**, calc. for $C_{23}H_{27}ClFIrN_4O_2$ 638.14358 $[M]^+$, found: 638.14662, **3d**, calc. for $C_{23}H_{23}ClF_5IrN_4O_2$ 710.10589 $[M + H]^+$, found: 710.10521, **3e**, calc. for $^1C_{23}H_{26}ClF_2IrN_4O_2$ 656.13416 $[M]^+$, found: 656.13608. Results from the elemental analysis of all iridium complexes also validate the proposed structural formulation.

On the other hand, the NHC–Ir(I) carbonyl derivatives (**4a–e**) were obtained by passing a stream of carbon monoxide through to a solution of the each one of the **3a–e** complexes. The **4a–e** complexes were obtained with yields ranging from 81% to 88%. The principal signals of the complexes correspond to the two-carbon monoxide (CO) molecules bonded to Ir(I), which appear in

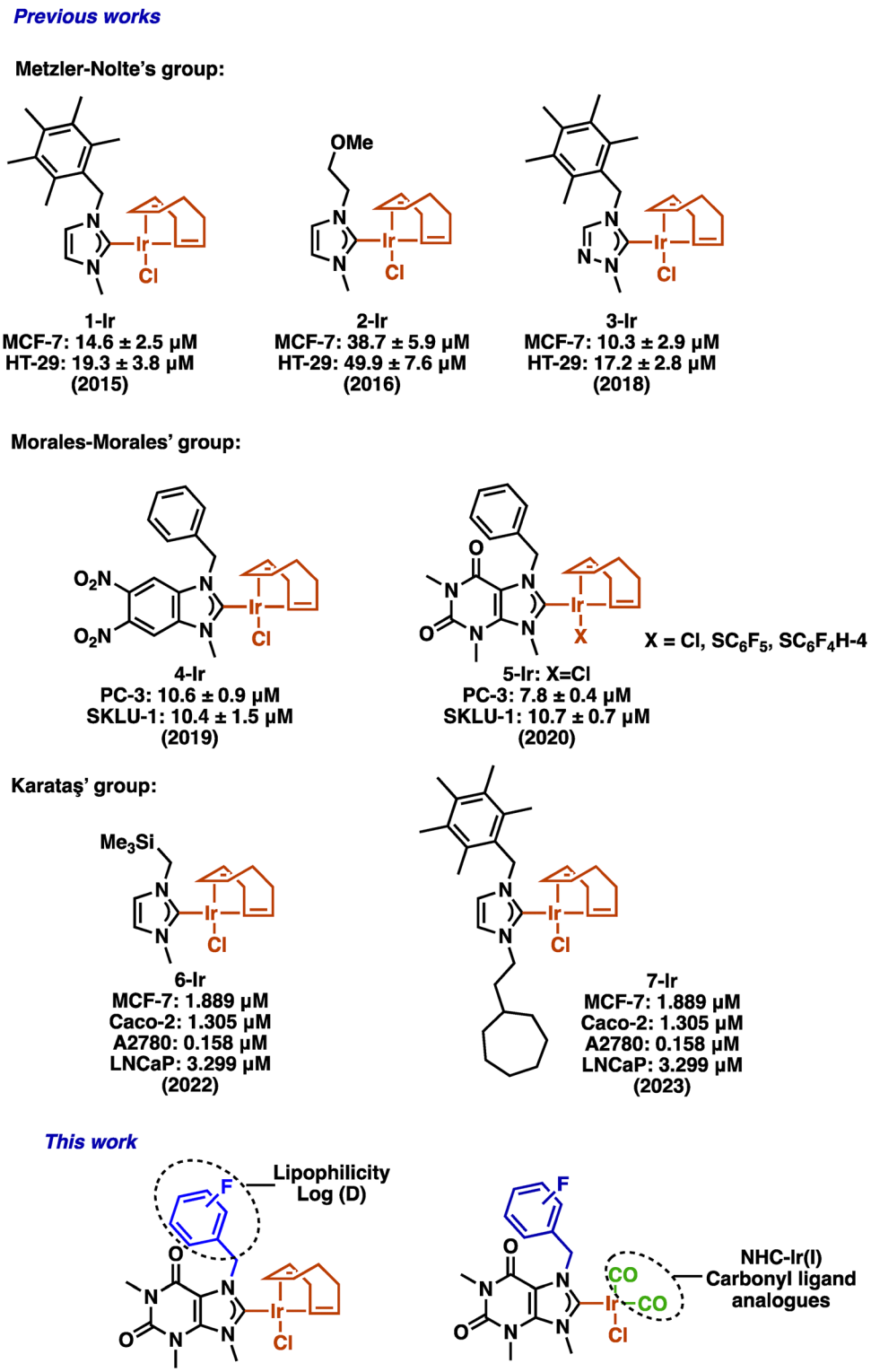

Fig. 1 Cytotoxic NHC–Ir(I) complexes: previous advances and new complexes with fluorinated NHC ligands and CO co-ligands.

the $^{13}C\{^{1}H\}$ NMR spectra between 166.9 to 180.2 ppm and the two bands in IR spectrum ($\tilde{\nu}$, cm^{-1}) between 2968.02 and 1973.34.

2.2. Cytotoxic evaluation

The cytotoxic activity of all compounds was initially evaluated in six human cancer cell lines: glioblastoma (U-251), chronic myelogenous leukemia (K-562), prostate adenocarcinoma (PC-3), colorectal adenocarcinoma (HCT-15), breast adenocarcinoma (MCF-7), and lung adenocarcinoma (SKLU-1). Additionally, healthy African green monkey kidney cells (COS-7) were included for comparison. This study aimed to assess the chemosensitivity of each cancer cell line to the synthesized compounds. The

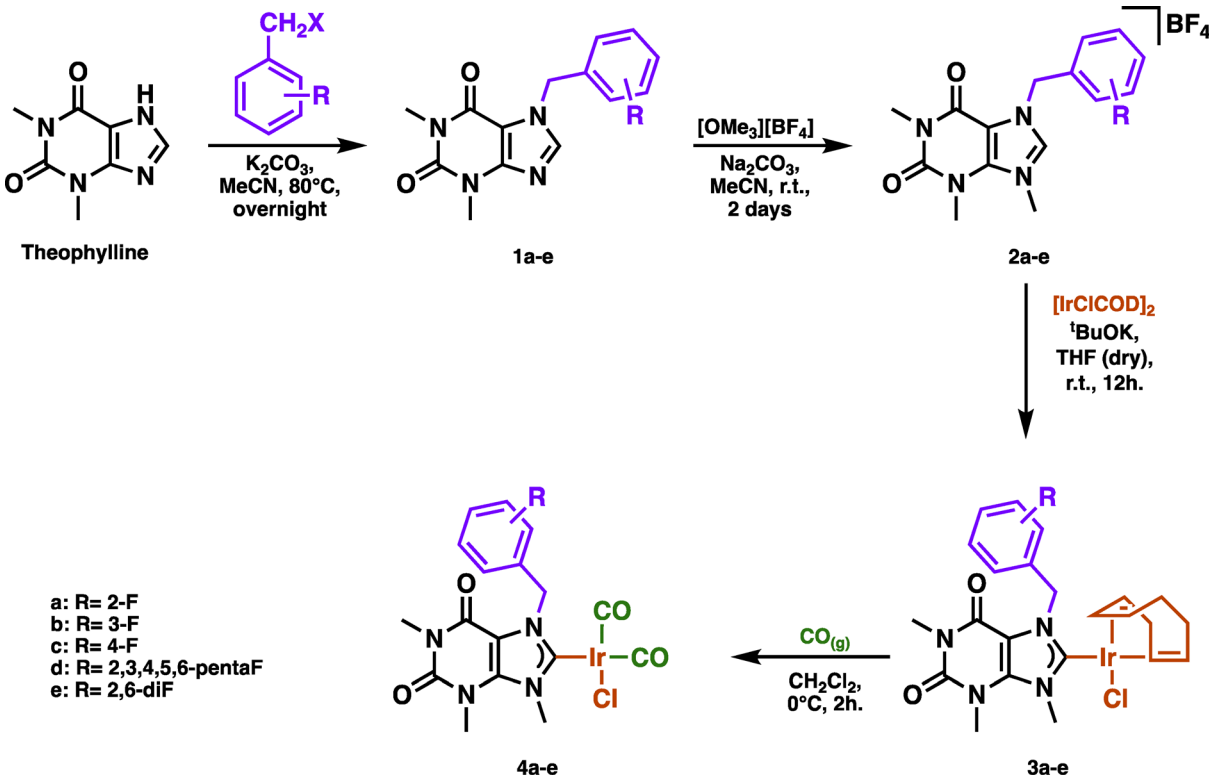

Scheme 1 Synthesis of azolium salts and their corresponding NHC–Ir(I) complexes.

results of this evaluation are summarized in Table S1 (ESI†). Overall, the results indicated that compounds **1a–e** and **2a–e**, along with the NHC–Ir(I) COD derivatives (**3a–e**), inhibited cell growth, while the NHC–Ir(I) carbonyl derivatives (**4a–e**) showed no cytotoxic activity in any of the cancer cell lines tested. These findings emphasize the critical role of ligand lability in the biological activity of these metal compounds. Specifically, the iridium complexes (**3a–e**) demonstrated superior activity compared to the azolium precursors (**1a–e**) and azolium salts (**2a–e**). Notably, all complexes **3a–e** (except **3d**) selectively inhibited cell growth in the leukemia cell line (K-562), with inhibition percentages ranging from 38.1% to 52.2%, while showing minimal inhibition in the non-cancerous COS-7 cell line (4.8–8.2%) (Table 1 and Fig. 2). In contrast, although compound **3d** exhibited the highest growth inhibition (68.2%) in the leukemia cell line, it was not selective and interfered with the growth of COS-7 cells (90.5%). Furthermore, complexes **3b** and **3c** also demonstrated promising results in inhibiting cell growth in the PC-3 and SKLU-1 cell lines. Based on these findings, the half-maximal inhibitory concentration (IC_{50}) values for the human cancer cell lines K-562, PC-3, and SKLU-1 are provided in Table 2.

The IC_{50} values of complexes **3a–3e** in K-562 cells ranged from 3.7 to 5.8 μM, which are lower than that of cisplatin (8.6 ± 0.9 μM). Notably, complexes **3a–3c** exhibited similar IC_{50} values, suggesting that the position of the fluorine substituent on the benzyl ring does not significantly impact cytotoxic activity. In contrast, complex **2e**, which is bi-fluorinated, displayed similar behavior to the mono-substituted derivatives (**3a–c**). Interestingly, the penta-fluorinated derivative (**3d**) showed the highest cytotoxic activity, with an IC_{50} value of 3.7 μM (Fig. 3), although its applicability is limited due to its activity in healthy cells (COS-7).

Complexes **3b** and **3c** exhibited similar potency against PC-3 cells, showing IC_{50} values between 5.1 and 5.7 μM, comparable to cisplatin. However, complex **3c** displayed lower potency than cisplatin in SKLU-1 cells (Fig. 4).

Table 1 Screening of cell growth inhibition (%) in K-562 and COS-7

Compound	K-562	COS-7
1a	4.0	10.1
1b	6.1	12.2
1c	22.2	11.7
1d	37.8	14.9
1e	28.4	13.9
2a	32.4	9.4
2b	22.2	9.7
2c	—	7.1
2d	3.8	7.1
2e	—	6.6
3a	38.1	5.5
3b	44.2	4.8
3c	50.6	5.9
3d	68.2	90.5
3e	52.2	8.2
4a	—	1.2
4b	—	3.0
4c	—	—
4d	—	0.6
4e	—	4.8

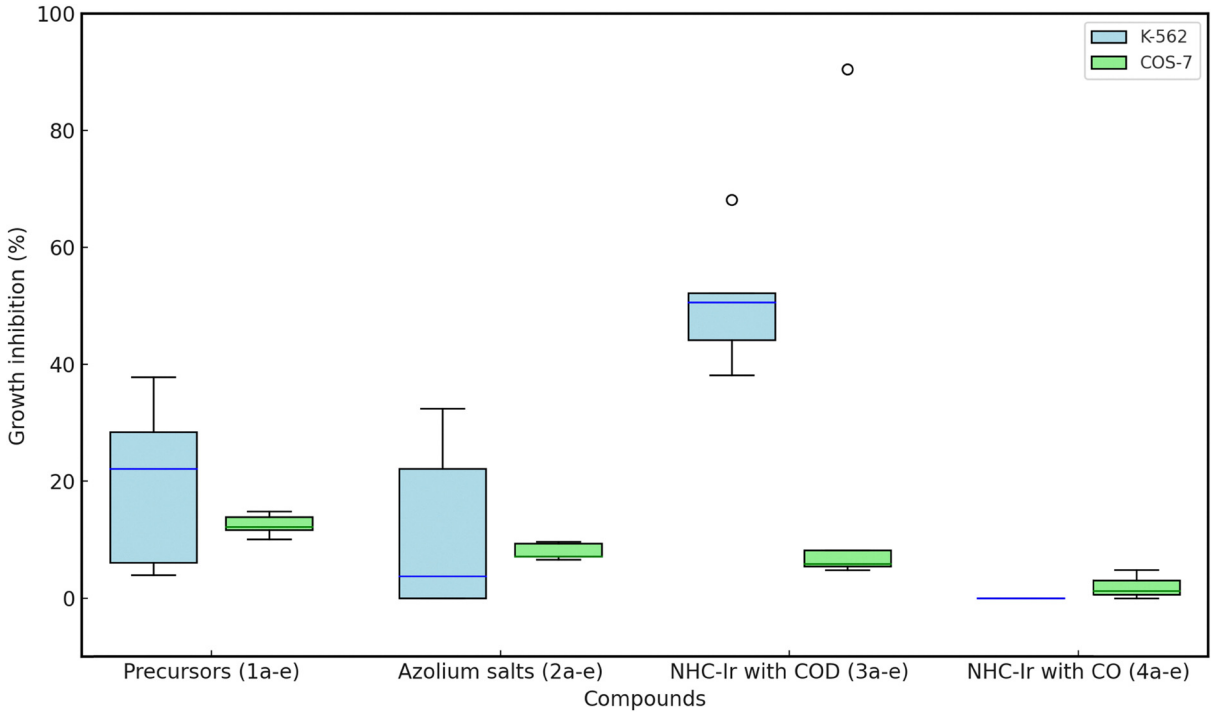

Fig. 2 Box plot comparison of the cytotoxic activity of the synthesized compounds.

Table 2 IC_{50} values obtained for NHC–Ir(I) complexes and cisplatin in μM against leukemia (K-562), prostatic adenocarcinoma (PC-3) and lung adenocarcinoma (SKLU-1)

	Complexes					
Cell line	**3a**	**3b**	**3c**	**3d**	**3e**	Cisplatin
K-562	5.1 ± 0.5	5.7 ± 0.6	5.4 ± 0.2	3.7 ± 0.6	5.8 ± 0.6	8.6 ± 0.9
PC-3	—	5.1 ± 0.9	5.7 ± 1.0	—	—	5.4 ± 0.8
SKLU-1	—	—	8.5 ± 0.7	—	—	4.3 ± 0.5

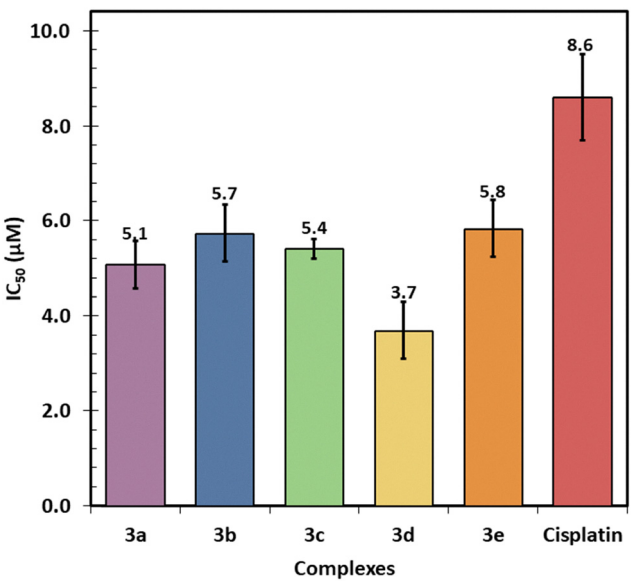

Fig. 3 IC_{50} (μM) of compounds against K-562 cell line.

2.3. Evaluation of the antioxidant properties of NHC–Ir(I) complexes

Metallodrugs, particularly those incorporating transition metal ions such as iridium, are promising candidates for cancer therapy due to their potential to generate reactive oxygen species (ROS). ROS are well known for inducing oxidative stress, ultimately leading to cancer cell death. Given the importance of this process and the ability of complexes **3a–e** to engage in relevant redox reactions, an evaluation was carried out to determine whether these compounds could generate ROS or act as antioxidant agents. This assessment was performed using the thiobarbituric acid reactive substances (TBARS) assay, in which ROS production is induced by $FeSO_4$ in the presence of lipids extracted from rat brain, Fig. 5.[27]

In this study, it was confirmed that the cytotoxic activity of the NHC–Ir(I) complexes (**3a–e**) is not dependent on the generation of reactive oxygen species (ROS). Instead, the complexes exhibited significant antioxidant activity (Table S4, ESI†), which may involve the oxidation of the metal center, leading to the formation of an active anticancer Ir(III) species through the loss of the COD ligand and chloride, as previously reported for iridium complexes bearing both ligands by oxidative addition with cytochrome *c* in the mitochondria.[28] The antioxidant activity of complexes **3a–e** ranged from 12.28 to 25.24 μM (Fig. 5). Among them, complex **3e**, featuring a bifluorinated structure, demonstrated the highest activity (IC_{50} = 12.28 ± 1.16 μM); however, its potency remained lower than that of the reference antioxidants α-tocopherol and BHT.

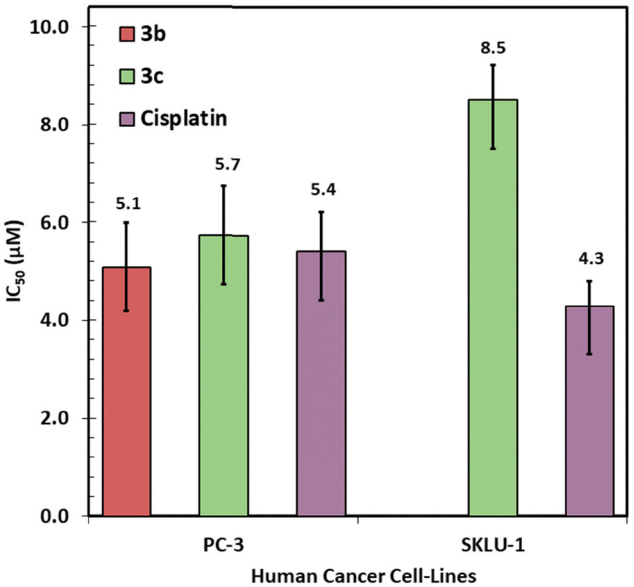

Fig. 4 Graph of IC_{50} (μM) of compounds (**3b** and **3c**) against PC-3 and SKLU-1.

In contrast, the NHC–Ir(I) carbonyl derivatives (**4a–e**) exhibited markedly lower antioxidant and cytotoxic activity (IC_{50} > 100 μM) compared to complexes **3a–e**, highlighting the critical role of labile ligands such as COD. This diminished activity may be attributed to the limited ability of the carbonyl complexes to undergo oxidation, which is necessary for the generation of the active Ir(III) species.

Overall, oxidative activation of the NHC–Ir(I) complexes (**3a–e**) plays an essential role in their cytotoxicity. Nevertheless, the absence of a direct correlation between antioxidant and cytotoxic activities within the **3a–e** complexes, along with the fact that antiproliferative effects occur at significantly lower concentrations than those required to elicit antioxidant activity, indicates the involvement of additional biological pathways.[29] These may include early mitochondrial stress as well as interactions with other intracellular targets, ultimately contributing to the overall antiproliferative response.

2.4. Electrochemical evaluation of NHC–Ir(I) complexes

To evaluate the redox behavior of the synthesized complexes and its potential correlation with their cytotoxic and antioxidant activities, electrochemical studies were conducted. The experiments were performed at a concentration of 0.1 mM in MeCN using an Autolab PGSTAT302N galvanostat/potentiostat in a three-electrode configuration: an Ag/AgCl reference electrode (saturated KCl, 3 M), a platinum wire as the counter electrode, and a glassy carbon electrode (GCE, ∅ = 3 mm) as the working electrode. A 0.1 M solution of tetra-*N*-butylammonium tetrafluoroborate (TBAF) was used as the supporting electrolyte. Ohmic drop compensation (*iR*) was applied using the current interrupt method.

The cyclic voltammetry results of the iridium complexes bearing COD (**3a–e**, Fig. 6a) and carbonyl (**4a–e**, Fig. 6b) ligands revealed distinct electrochemical behaviors. Complexes **3a–e** exhibited an irreversible electrochemical profile with a well-defined anodic peak corresponding to the oxidation of Ir(I) to Ir(III), occurring between 0.92 and 1.10 V, with no corresponding cathodic peak observed. In contrast, complexes **4a–e** showed a broad, irreversible anodic peak associated with the oxidation of Ir(I) to Ir(III) at higher potentials, ranging from 1.49 to 1.72 V. This shift is attributed to the electron-withdrawing nature of the CO ligands, which reduce electron density at the metal center. The lower oxidation potentials observed for the COD-containing complexes (**3a–e**) suggest a more favorable oxidation process to Ir(III), which correlates with their enhanced biological activity profiles.

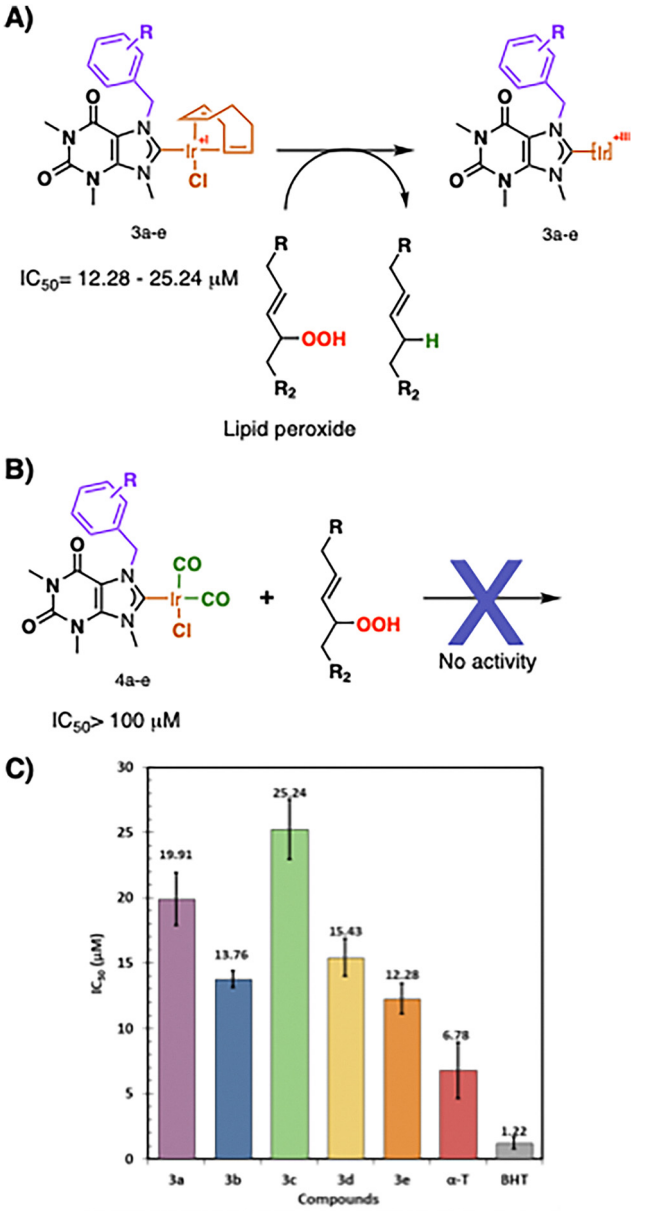

Fig. 5 Antioxidant activity. (A) Complexes **3a–e** react with lipid peroxides *via* a redox process, likely involving oxidative activation. (B) Carbonyl analogues **4a–e** remain inactive (IC_{50} > 100 μM), suggesting CO ligands inhibit redox activation. (C) Graph of IC_{50} (μM) for the complexes (**3a–e**).

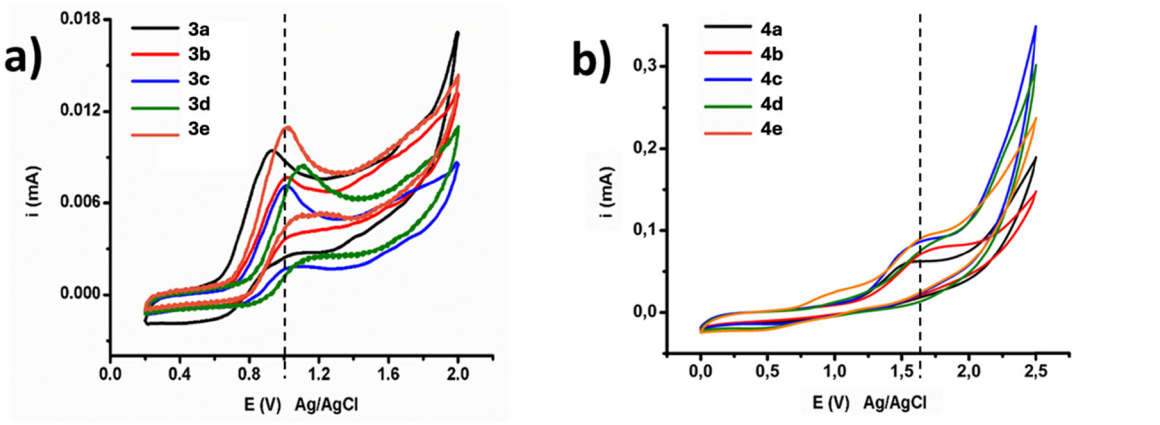

$Ir^{I}L \rightarrow Ir^{III}L$	3a	3b	3c	3d	3e
Ep_a (V)	0.92	1.00	1.01	1.10	0.99

$Ir^{I}L \rightarrow Ir^{III}L$	4a	4b	4c	4d	4e
Ep_a (V)	1.49	1.64	1.56	1.72	1.61

Fig. 6 Cyclic Voltammograms of the NHC–Ir(I) complexes. (a) **3a–e** complexes and (b) **4a–e** complexes.

2.5. Determination of the partition coefficient log(*D*) pH 7.4 of the NHC–Ir(I) complexes

The ability of metal complexes to partition between lipid and aqueous media is of paramount importance in drug development, as it provides insights into a compound's capacity to traverse biological membranes, dissolve in lipid-rich tissues or aqueous environments, and achieve effective absorption within an organism. Accordingly, the partition coefficient (log *D*) of complexes **3a–3e** was determined using a physiological phosphate buffer solution at pH 7.4 and *n*-octanol, following the shake-flask method. Quantification was carried out by high-performance liquid chromatography (HPLC) according to procedure **1b** reported by J. M. Huerta.[30] For this assay, the stock solutions of the complexes were prepared using MeCN instead of DMSO.

The log *D* values of complexes **3a–3e** are summarized in Table 3 and range from 2.87 to 3.95. In general, an increase in lipophilicity was observed with the progressive addition of fluorine atoms to the benzyl fragment. In this regard, the pentafluorinated derivative (**3d**) exhibited the highest log *D* value (3.95). Conversely, the position of the fluorine substituent in the monosubstituted compounds (**3a–3c**) had only a minor influence on their partition coefficients. The log *D* value for complex **3c** (2.87) suggests that it maintains an adequate balance between water solubility and membrane permeability, both critical factors for bioavailability and therapeutic efficacy, as reflected in the cytotoxicity assays. However, the log *D* values of the remaining complexes exceeded 3.00, which may serve as a cautionary indicator. Compounds with log *D* values between 3 and 5 are often associated with reduced aqueous solubility and may be more susceptible to metabolic transformations.[30]

Table 3 Partition coefficient (log *D* o/w) of the NHC–Ir(I) complexes

	Complexes				
	3a	**3b**	**3c**	**3d**	**3e**
Log *D*	3.42	3.73	2.87	3.95	3.74

Interestingly, although complexes **3a**, **3b**, **3d**, and **3e** exhibited higher log *D* values (>3.4), their cytotoxic activity was comparable to that of **3c** (log *D* = 2.87), suggesting that lipophilicity alone does not strictly dictate cytotoxic activity in this series. Given that mitochondrial disruption is a proposed mechanism of action, efficient permeability of both the cellular and mitochondrial membranes is essential. Therefore, it is proposed that these complexes may be internalized (cellular uptake) through analogous mechanisms to drug delivery systems, such as endocytosis mediated by clathrin or caveolin and direct translocation.[29] These pathways could allow the compounds to reach the cytoplasm, and subsequently interact with mitochondrial targets such as cytochrome *c*, contributing to their cytotoxic effects.

3. Conclusions

In summary, a series of Ir(I)–NHC complexes derived from theophylline, featuring varying degrees and positions of fluorine substitution on the benzyl ring, were successfully synthesized and characterized. While the free ligands exhibited no inherent cytotoxicity, their coordination to Ir(I) centers with COD ligands yielded NHC–Ir(I) complexes (**3a–e**) with notable anticancer activity, particularly against the K-562 leukemia cell line (IC_{50}: 3.7–5.8 μM), surpassing the performance of cisplatin (IC_{50}: 8.6 ± 0.9 μM). The observed cytotoxicity appears to be closely associated with the formation of active Ir(III) species, as supported by antioxidant assays and electrochemical studies, underscoring the essential role of the oxidation process in the mechanism of action.

Among all the compounds tested, complex **3c** emerged as the most potent anticancer agent, exhibiting significant activity against K-562, PC-3, and SKLU-1 cancer cell lines, with IC_{50} values of 5.4 ± 0.2, 5.7 ± 1.0, and 8.5 ± 0.7 μM, respectively,

while showing minimal cytotoxicity toward healthy COS-7 cells. This favorable biological profile, combined with its optimal balance between aqueous solubility and membrane permeability ($\log D$ = 2.87), highlights complex **3c** as a strong candidate for further investigation. Ongoing studies in our laboratory aim to build upon these findings and assess its potential in preclinical models.

4. Experimental

4.1. Materials

All reagents were commercially obtained and used as received without further purification. The ^{1}H and ^{13}C{1H} NMR spectra were recorded on a Bruker Ascend 500 spectrometer. Chemical shifts are reported in ppm down field of TMS using the residual signals in the solvent as internal standard. Elemental analyses were performed on a PerkinElmer 240. CHNS analyses were performed in Thermo Scientific Flash 2000 elemental analyzed, using a Mettler Toledo XP6 Automated-S Microbalance and sulfanilamide as standard (Thermo Scientific BN 217826, attained values N = 16.40%, C = 41.91%, H = 4.65% and S = 18.63%; certified values N = 16.26%, C = 41.81%, H = 4.71% and S = 18.62%). MS-electrospray determinations were recorded on a Bruker Daltonics-Esquire 3000 plus electrospray mass spectrometer.

4.2. Methods

4.2.1. General procedure for the synthesis of *N*-substituted-theophylline (1a–e). In a typical experiment, 1.05 equivalents of the corresponding benzyl halide were added to a mixture of theophylline (1.0 equiv.) and K_2CO_3 (1.05 equiv.) in acetonitrile (100 mL). The reaction mixture was stirred and heated at 80 °C overnight. After cooling to room temperature, the mixture was filtered through Celite®. The volatiles were then removed under high vacuum, and the crude product was washed three times with diethyl ether.

*7-(2-Fluorobenzyl)-1,3-dimethyl-3,7-dihydro-1H-purine-2,6-dione (**1a**).* For the synthesis of (**1a**) was used 2-fluorobenzyl chloride (347 μL, 2.91 mmol), theophylline (500 mg, 2.78 mmol) and K_2CO_3 (403 mg, 2.91 mmol). Yield: 636 mg (79.4%). ^{1}H NMR (500 MHz, $CDCl_3$) δ 7.66 (s, 1H, NCHN), 7.53–7.50 (m, 1H, CH_{Ar}), 7.35–7.31 (m, 1H, CH_{Ar}), 7.15–7.06 (m, 2H), 5.56 (s, 2H, –CH_2–), 3.57 (s, 6H, –CH_3), 3.40 (s, 6H, –CH_3). ^{13}C{^{1}H} NMR (126 MHz, $CDCl_3$) δ 161.0 (d, $^{1}J_{C-F}$ = 247.3 Hz, CF_{Ar}), 155.4 (C═O), 151.8 (C═O), 148.9 ($C_{theophy}$), 141.6 (NCHN), 131.2–131.1 (CH_{Ar}), 131.0–130.9 (CH_{Ar}), 124.9 (CH_{Ar}), 122.9–122.8 (C_{Ar}), 115.9–115.7 (CH_{Ar}), 106.9 ($C_{theophy}$), 44.1 (–CH_2–), 29.9 (–CH_3), 28.2 (–CH_3). ^{19}F NMR (282 MHz, $CDCl_3$) δ −118.24 (CF_{Ar}). MS (DART^{+}): *m*/*z* 289 [M + H]$^{+}$. Elem. anal. calcd for $C_{14}H_{13}FN_4O_2$: C, 58.33; H, 4.55; N, 19.44. Found: C, 58.59; H, 4.31; N, 19.46. Melting point: 141.0–143.2 °C. HPLC relative purity: 98.71%.

*7-(3-Fluorobenzyl)-1,3-dimethyl-3,7-dihydro-1H-purine-2,6-dione (**1b**).* For the synthesis of (**1b**) was used 3-fluorobenzyl bromide (357 μL, 2.91 mmol), theophylline (500 mg, 2.78 mmol) and K_2CO_3 (403 mg, 2.91 mmol). Yield: 602 mg (75.2%). ^{1}H NMR (500 MHz, $CDCl_3$): δ 7.59 (s, 1H, NCHN), 7.38–7.31 (m, 1H, CH_{Ar}), 7.10–7.08 (m, 1H, CH_{Ar}), 7.04–6.98 (m, 2H, CH_{Ar}), 5.49 (s, 2H, –CH_2–), 3.58 (s, 3H, –CH_3), 3.39 (s, 3H, –CH_3). ^{13}C{^{1}H} NMR (126 MHz, $CDCl_3$) δ 163.1 (d, $^{1}J_{C-F}$ = 247.7 Hz, CF_{Ar}), 155.4 (C═O), 151.8 (C═O), 149.0 ($C_{theophy}$), 141.0 (NCHN), 138.0–137.9 (C_{Ar}), 130.9–130.8 (CH_{Ar}), 123.5 (CH_{Ar}), 115.9–115.7 (CH_{Ar}), 115.0–114.8 (CH_{Ar}), 107.0 ($C_{theophy}$), 49.8 (–CH_2–), 29.9 (–CH_3), 28.2 (–CH_3). ^{19}F NMR (282 MHz, $CDCl_3$) δ −111.58 (CF_{Ar}). MS (DART^{+}): *m*/*z* 289 [M + H]$^{+}$. Elem. anal. calcd for $C_{14}H_{13}FN_4O_2$: C, 58.33; H, 4.55; N, 19.44. Found: C, 58.43; H, 4.32; N, 19.49. Melting point: 173.5–175.1 °C. HPLC relative purity: 99.93%.

*7-(4-Fluorobenzyl)-1,3-dimethyl-3,7-dihydro-1H-purine-2,6-dione (**1c**).* For the synthesis of (**1c**) was used 4-fluorobenzyl chloride (346 μL, 2.91 mmol), theophylline (500 mg, 2.78 mmol) and K_2CO_3 (403 mg, 2.91 mmol). Yield: 662 mg (82.7%). ^{1}H NMR (500 MHz, $CDCl_3$) δ 7.57 (s, 1H, NCHN), 7.35–7.31 (m, 2H, CH_{Ar}), 7.07–7.02 (m, 2H, CH_{Ar}), 5.46 (s, 1H, –CH_2–), 3.57 (s, 1H, –CH_3), 3.40 (s, 1H, –CH_3). ^{13}C{^{1}H} NMR (126 MHz, $CDCl_3$) δ 162.8 (d, $^{1}J_{C-F}$ = 247.9 Hz, CF_{Ar}), 155.3 (C═O), 151.6 (C═O), 149.0 ($C_{theophy}$), 140.7 (NCHN), 131.3–131.2 (C_{Ar}), 129.9 (2 × CH_{Ar}), 116.2–116.0 (2 × CH_{Ar}), 106.9 ($C_{theophy}$), 49.6 (–CH_2–), 29.8 (–CH_3), 28.0 (–CH_3). ^{19}F NMR (282 MHz, $CDCl_3$) δ −112.82 (CF_{Ar}). MS (DART^{+}): *m*/*z* 289 [M + H]$^{+}$. Elem. anal. calcd for $C_{14}H_{13}FN_4O_2$: C, 58.33; H, 4.55; N, 19.44. Found: C, 58.54; H, 4.68; N, 19.51. Melting point: 203.4–205.1 °C. HPLC relative purity: 99.68%.

*1,3-Dimethyl-7-((perfluorophenyl)methyl)-3,7-dihydro-1H-purine-2,6-dione (**1d**).* For the synthesis of (**1d**) was used 2,3,4,5,6-pentafluorobenzyl bromide (440 μL, 2.91 mmol), theophylline (500 mg, 2.78 mmol) and K_2CO_3 (403 mg, 2.91 mmol). Yield: 748 mg (74.7%). ^{1}H NMR (500 MHz, $CDCl_3$) δ 7.60 (s, 1H, NCHN), 5.65 (s, 2H, –CH_2–), 3.57 (s, 3H, –CH_3), 3.38 (s, 3H, –CH_3). ^{13}C{^{1}H} NMR (126 MHz, $CDCl_3$) δ 155.2 (C═O), 151.7 (C═O), 148.8 ($C_{theophy}$), 146.7 (CF_{Ar}), 144.7 (CF_{Ar}), 143.1 (CF_{Ar}), 141.4 (NCHN), 141.0 (CF_{Ar}), 138.8 (CF_{Ar}), 136.8 (CF_{Ar}), 109.2–108.9 (C_{Ar}), 107.0 ($C_{theophy}$), 38.2 (–CH_2–), 29.9 (–CH_3), 28.2 (–CH_3). ^{19}F NMR (282 MHz, $CDCl_3$) δ −141.42 (CF_{Ar}), −151.36 (CF_{Ar}), −160.23 (CF_{Ar}). MS (DART^{+}): *m*/*z* 361 [M + H]$^{+}$. Elem. anal. calcd for $C_{14}H_9F_5N_4O_2$: C, 46.68; H, 2.52; N, 15.55. Found: C, 46.91; H, 2.48; N, 15.51. Melting point: 155.4–157.5 °C. HPLC relative purity: 99.80%.

*7-(2,6-Difluorobenzyl)-1,3-dimethyl-3,7-dihydro-1H-purine-2,6-dione (**1e**).* For the synthesis of (**1e**) was used 2,6-difluorobenzyl chloride (474 mg, 2.91 mmol), theophylline (500 mg, 2.78 mmol) and K_2CO_3 (403 mg, 2.91 mmol). Yield: 743 mg (87.4%). ^{1}H NMR (500 MHz, $CDCl_3$) δ 7.49 (s, 1H, NCHN), 7.40–7.34 (m, 1H, CH_{Ar}), 7.00–6.94 (m, 2H, CH_{Ar}), 5.65 (s, 2H, –CH_2–), 3.57 (s, 1H, –CH_3), 3.41 (s, 1H, –CH_3). ^{13}C{^{1}H} NMR (126 MHz, $CDCl_3$) δ 161.6 (d, $^{1}J_{C-F}$ = 251.4 Hz, CF_{Ar}), 155.4 (C═O), 151.8 (C═O), 148.6 ($C_{theophy}$), 141.1 (NCHN), 131.6–131.4 (CH_{Ar}), 112.1–111.9 (CH_{Ar}), 111.3–111.0 (C_{Ar}), 107.3 ($C_{theophy}$), 38.2 (–CH_2–), 29.9 (–CH_3), 28.2 (–CH_3). ^{19}F NMR (282 MHz, $CDCl_3$) δ −113.65 (CF_{Ar}). MS (DART^{+}): *m*/*z* 307 [M + H]$^{+}$. Elem. anal.

calcd for $C_{14}H_{12}F_2N_4O_2$: C, 54.90; H, 3.95; N, 18.29. Found: C, 55.36; H, 3.78; N, 18.50. Melting point: 173.7–175.4 °C. HPLC relative purity: 95.58%.

4.2.2. General procedure for the synthesis of azolium salts derived of theophylline (2a–e). To a solution of functionalized theophylline (**1a–e**) in acetonitrile (25 mL), trimethyloxonium tetrafluoroborate (1.05 equiv.) and Na_2CO_3 (1.05 equiv.) were added. The mixture was stirred at room temperature overnight. After this period, the reaction progress was monitored by TLC using hexane : ethyl acetate (1 : 1) as the mobile phase, which indicated incomplete conversion. Consequently, an additional portion of trimethyloxonium tetrafluoroborate (0.6 equiv.) was added, and stirring was continued for another 24 hours. The resulting mixture was then filtered through Celite®, and all volatiles were removed under high vacuum. The crude product was purified by crystallization from hot methanol.

Azolium salt (2a). For the synthesis of (**2a**) was used (**1a**) (288 mg, 1.0 mmol), Na_2CO_3 (100 mg, 1.05 mmol) and trimethyloxonium tetrafluoroborate (155 mg, 1.05 mmol + 89 mg, 0.60 mmol). Yield: 351 mg (90.1%). ^{1}H NMR (400 MHz, DMSO-d_6) δ 9.41 (s, 1H, NCHN), 7.51–7.43 (m, 2H, CH_{Ar}), 7.34–7.23 (m, 2H, CH_{Ar}), 5.78 (s, 2H, –CH_2–), 4.17 (s, 3H, –CH_3), 3.73 (s, 3H, –CH_3), 3.25 (s, 3H. –CH_3). ^{13}C{^{1}H} NMR (101 MHz, DMSO-d_6) δ 160.20 (d, $^1J_{C-F}$ = 247.1 Hz, CF_{Ar}), 153.0 (C═O), 150.1 (C═O), 139.9 ($C_{theophy}$), 139.8 (NCHN), 131.4–131.3 (CH_{Ar}), 130.5 (CH_{Ar}), 124.9 (CH_{Ar}), 121.0–120.9 (C_{Ar}), 115.8–115.6 (CH_{Ar}), 107.1 ($C_{theophy}$), 45.8 (–CH_2–), 37.1 (–CH_3), 31.3 (–CH_3), 28.5 (–CH_3). ^{19}F NMR (282 MHz, DMSO-d_6) δ −116.94 (CF_{Ar}), −148.42 (BF_4). MS (DART$^+$): *m*/*z* 303 [M − BF_4]$^+$. Elem. anal. calcd for $C_{15}H_{16}BF_5N_4O_2$: C, 46.18; H, 4.13; N, 14.36. Found: C, 46.26; H, 4.18; N, 14.66. Melting point: 228.7–230.4 °C. HPLC relative purity: 98.28%.

Azolium salt (2b). For the synthesis of (**2b**) was used (**1b**) (288 mg, 1.0 mmol), Na_2CO_3 (100 mg, 1.05 mmol) and trimethyloxonium tetrafluoroborate (155 mg, 1.05 mmol + 89 mg, 0.60 mmol). Yield: 345 mg (88.5%). ^{1}H NMR (400 MHz, DMSO-d_6) δ 9.28 (s, 1H, NCHN), 7.76–7.74 (m, 1H, CH_{Ar}), 7.44–7.34 (m, 2H, CH_{Ar}), 7.20–7.18 (m, 1H, CH_{Ar}), 5.77 (s, 2H, –CH_2–), 4.17 (s, 3H, –CH_3), 3.75 (s, 3H, –CH_3), 3.23 (s, 3H, –CH_3). ^{13}C{^{1}H} NMR (101 MHz, DMSO-d_6) δ 160.35 (d, $^1J_{C-F}$ = 246.9 Hz, CF_{Ar}), 153.0 (C═O), 150.2 (C═O), 139.9 ($C_{theophy}$), 139.8 (NCHN), 133.0–132.9 (CH_{Ar}), 130.7 (CH_{Ar}), 129.2 (CH_{Ar}), 128.3 (CH_{Ar}), 122.3 (C_{Ar}), 107.3 ($C_{theophy}$), 51.6 (–CH_2–), 37.1 (–CH_3), 31.3 (–CH_3), 28.4 (–CH_3). ^{19}F NMR (376 MHz, acetone-d_6) δ −113.64 (CF_{Ar}), −151.69 (BF_4). MS (DART$^+$): *m*/*z* 303 [M − BF_4]$^+$. Elem. anal. calcd for $C_{15}H_{16}BF_5N_4O_2$: C, 46.18; H, 4.13; N, 14.36. Found: C, 46.31; H, 4.20; N, 14.51. Melting point: 246.0–249.0 °C. HPLC relative purity: 97.77%.

Azolium salt (2c). For the synthesis of (**2c**) was used (**1c**) (288 mg, 1.0 mmol), Na_2CO_3 (100 mg, 1.05 mmol) and trimethyloxonium tetrafluoroborate (155 mg, 1.05 mmol + 89 mg, 0.60 mmol). Yield: 363 mg (93.0%). ^{1}H NMR (400 MHz, DMSO-d_6) δ 9.42 (s, 1H, NCHN), 7.55–7.50 (m, 2H, CH_{Ar}), 7.29–7.23 (m, 2H, CH_{Ar}), 5.69 (s, 2H, –CH_2–), 4.14 (s, 3H, –CH_3), 3.72 (s, 3H, –CH_3), 3.26 (s, 3H, –CH_3). ^{13}C{^{1}H} NMR (101 MHz, DMSO-d_6) δ 162.28 (d, $^1J_{C-F}$ = 245.4 Hz, CF_{Ar}), 153.1 (C═O), 150.1 (C═O), 139.9 ($C_{theophy}$), 139.4 (NCHN), 130.8–130.7 (2 × CH_{Ar}), 130.3–130.2 (C_{Ar}), 115.8–115.6 (2 × CH_{Ar}), 106.9 ($C_{theophy}$), 50.4 (–CH_2–), 37.1 (–CH_3), 31.3 (–CH_3), 28.5 (–CH_3). ^{19}F NMR (282 MHz, DMSO-d_6) δ −112.98 (CF_{Ar}), −148.40 (BF_4). MS (DART$^+$): *m*/*z* 303 [M − BF_4]$^+$. Elem. anal. calcd for $C_{15}H_{16}BF_5N_4O_2$: C, 46.18; H, 4.13; N, 14.36. Found: C, 46.20; H, 4.22; N, 14.59. Melting point: 268.7–270.1 °C. HPLC relative purity: 97.77%.

Azolium salt (2d). For the synthesis of (**2d**) was used (**1d**) (360 mg, 1.0 mmol), Na_2CO_3 (100 mg, 1.05 mmol) and trimethyloxonium tetrafluoroborate (155 mg, 1.05 mmol + 89 mg, 0.60 mmol). Yield: 421 mg (91.2%). ^{1}H NMR (700 MHz, DMSO-d_6) δ 9.41 (s, 1H, NCHN), 5.89 (s, 2H, –CH_2–), 4.16 (s, 3H, –CH_3), 3.73 (s, 3H, –CH_3), 3.26 (s, 3H, –CH_3). ^{13}C{^{1}H} NMR (176 MHz, DMSO-d_6) δ 153.1 (C═O), 150.0 (C═O), 146.1 (CF_{Ar}), 144.7–144.6 (CF_{Ar}), 142.0 (CF_{Ar}), 140.3 ($C_{theophy}$), 139.6 (NCHN), 137.7 (CF_{Ar}), 136.3 (CF_{Ar}), 107.7–107.5 (CAr), 107.3 ($C_{theophy}$), 40.3 (–CH_2–), 37.1 (–CH_3), 31.3 (–CH_3), 28.5 (–CH_3). ^{19}F NMR (282 MHz, DMSO-d_6) δ −140.09 (CF_{Ar}), −112.98 (CF_{Ar}) −148.35 (BF_4), −152.64 (CF_{Ar}), −162.18 (CF_{Ar}). MS (DART$^+$): *m*/*z* 375 [M − BF_4]$^+$. Elem. anal. calcd for $C_{15}H_{12}BF_9N_4O_2$: C, 38.99; H, 2.62; N, 12.13. Found: C, 38.72; H, 2.22; N, 12.61. Melting point: 201.0–203.0 °C. HPLC relative purity: 97.55%.

Azolium salt (2e). For the synthesis of (**2e**) was used (**1e**) (306 mg, 1.0 mmol), Na_2CO_3 (100 mg, 1.05 mmol) and trimethyloxonium tetrafluoroborate (155 mg, 1.05 mmol + 89 mg, 0.60 mmol). Yield: 389 mg (95.4%). ^{1}H NMR (400 MHz, DMSO-d_6) δ 9.36 (s, 1H, NCHN), 7.61–7.54 (m, 1H, CH_{Ar}), 7.25–7.19 (m, 2H, CH_{Ar}), 5.81 (s, 2H, –CH_2–), 4.14 (s, 3H, –CH_3), 3.71 (s, 3H, –CH_3), 3.25 (s, 2H, –CH_3). ^{13}C{^{1}H} NMR (101 MHz, DMSO-d_6) δ 161.01 (d, $^1J_{C-F}$ = 250.5 Hz, 2 × CF_{Ar}), 153.0 (C═O), 150.1 (C═O), 139.8 ($C_{theophy}$), 139.6 (NCHN), 132.6–132.4 (CH_{Ar}), 112.1 (2 × CH_{Ar}), 109.3–109.0 (C_{Ar}), 107.3 ($C_{theophy}$), 40.6 (–CH_2–), 36.9 (–CH_3), 31.2 (–CH_3), 28.5 (–CH_3). ^{19}F NMR (282 MHz, DMSO-d_6) δ −112.96 (CF_{Ar}), −148.37 (BF_4). MS (DART$^+$): *m*/*z* 321 [M − BF_4]$^+$. Elem. anal. calcd for $C_{15}H_{15}BF_6N_4O_2$: C, 44.15; H, 3.70; N, 13.73. Found: C, 44.20; H, 3.62; N, 14.01. Melting point: 318.7–320.1 °C. HPLC relative purity: 96.12%.

4.2.3. General procedure for the synthesis of Ir(I)–NHC complexes with COD (3a–e). In a Schlenk flask, $[IrCl(COD)]_2$ (1 equiv.), potassium *tert*-butoxide (2.05 equiv.), and the corresponding azolium salt (**2a–e**) (2 equiv.) were combined. The flask was subjected to alternating nitrogen purges to ensure an inert atmosphere. Subsequently, dry THF (15 mL) was added in a single portion to the solid mixture, and the reaction was stirred overnight at room temperature under nitrogen. After this time, the mixture was filtered through Celite®, and all volatiles were removed under high vacuum. The crude product was purified by column chromatography using hexane : ethyl acetate (2 : 1) as the mobile phase, affording a yellow band corresponding to the desired product.

*Complex (**3a**).* For the synthesis of (**3a**) was used $[IrClCOD]_2$ (168 mg, 0.25 mmol), potassium *tert*-butoxide (58 mg, 0.51 mmol) and (**2a**) (195 mg, 0.50 mmol). Yield: 154 mg (48.2%). ^{1}H NMR (500 MHz, $CDCl_3$) δ 7.25–7.22 (m, 1H, CH_{Ar}), 7.17–7.02 (m, 3H, CH_{Ar}), 6.16 (d, $^2J_{H-H}$ = 15.3 Hz, 1H, –CH_2–), 6.06 (d, $^2J_{H-H}$ = 15.4 Hz, 1H, –CH_2–), 4.82–4.79 (m, 1H, CH_{COD}), 4.72–4.68 (m, 1H, CH_{COD}), 4.50 (s, 3H, –CH_3), 3.81 (s, 3H, –CH_3), 3.29 (s, 3H, –CH_3), 2.96–2.93 (m, 1H, CH_{COD}), 2.65–2.62 (m, 1H, CH_{COD}), 2.31–2.12 (m, 3H, CH_{2COD}), 2.00–1.93 (m, 1H, CH_{2COD}), 1.89–1.82 (m, 1H, CH_{2COD}), 1.77–1.67 (m, 2H, CH_{2COD}), 1.50–1.43 (m, 1H, CH_{2COD}). $^{13}C\{^1H\}$ NMR (126 MHz, $CDCl_3$) δ 189.0 (C_{NHC-Ir}), 160.14 (d, $^1J_{C-F}$ = 247.2 Hz, CF_{Ar}), 152.4 (C═O), 150.7 (C═O), 140.7 ($C_{theophy}$), 129.4–129.3 (CH_{Ar}), 128.2 (CH_{Ar}), 124.4 (CH_{Ar}), 124.2–124.1 (C_{Ar}), 115.5–115.3 (CH_{Ar}), 109.6 ($C_{theophy}$), 89.0 (CH_{COD}), 87.8 (CH_{COD}), 53.4 (CH_{COD}), 52.7 (CH_{COD}), 47.1–47.0 (–CH_2–), 39.1 (–CH_3), 34.5 (CH_{2COD}), 32.6 (CH_{2COD}), 32.0 (–CH_3), 30.0 (CH_{2COD}), 28.7 (CH_{2COD}), 28.6 (–CH_3). ^{19}F NMR (376 MHz, $CDCl_3$) δ −117.96 (CF_{Ar}). HR-MS electrospray ($DART^+$): calc. mass: 638.14358 *m*/*z* for $^{12}C_{23}{}^1H_{27}{}^{35}Cl_1{}^{19}F_1{}^{193}Ir_1{}^{14}N_4{}^{16}O_2$ $[M]^+$. Found: 638.14547 *m*/*z*. Mass difference: 2.96 ppm. Elem. anal. calcd for $C_{23}H_{27}ClFIrN_4O_2$: C, 43.29; H, 4.26; N, 8.78. Found: C, 43.20; H, 4.22; N, 8.59. Melting point: 184.0–186.1 °C. HPLC relative purity: 96.79%.

*Complex (**3b**).* For the synthesis of (**3b**) was used $[IrClCOD]_2$ (168 mg, 0.25 mmol), potassium *tert*-butoxide (58 mg, 0.51 mmol) and (**2b**) (195 mg, 0.50 mmol). Yield: 165 mg (51.8%). ^{1}H NMR (500 MHz, $CDCl_3$) δ 7.31–7.27 (m, 2H, CH_{Ar}), 7.20–7.17 (m, 1H, CH_{Ar}), 6.98–6.94 (m, 1H, CH_{Ar}), 6.10 (d, $^2J_{H-H}$ = 14.7 Hz, 1H, –CH_2–), 5.91 (d, $^2J_{H-H}$ = 14.8 Hz, 1H, –CH_2–), 4.87–4.84 (m, 1H, CH_{COD}), 4.74–4.70 (m, 1H, CH_{COD}), 4.49 (s, 3H, –CH_3), 3.80 (s, 3H, –CH_3), 3.32 (s, 3H, –CH_3), 2.94–2.90 (m, 1H, CH_{COD}), 2.59–2.55 (m, 1H, CH_{COD}), 2.32–2.14 (m, 3H, CH_{2COD}), 1.99–1.87 (m, 2H, CH_{2COD}), 1.78–1.66 (m, 2H, CH_{2COD}), 1.49–1.42 (m, 1H, CH_{2COD}). $^{13}C\{^1H\}$ NMR (126 MHz, $CDCl_3$) δ 188.9 (C_{NHC-Ir}), 162.93 (d, $^1J_{C-F}$ = 245.9 Hz, CF_{Ar}), 152.6 (C═O), 150.7 (C═O), 140.9 ($C_{theophy}$), 139.2–139.1 (C_{Ar}), 130.2–130.1 (CH_{Ar}), 123.5 (CH_{Ar}), 115.0 (CH_{Ar}), 114.8 (CH_{Ar}), 109.6 ($C_{theophy}$), 88.9 (CH_{COD}), 87.9 (CH_{COD}), 53.7 (CH_{COD}), 52.9 (CH_{COD}), 52.7 (–CH_2–), 39.2 (–CH_3), 34.5 (CH_{2COD}), 32.5 (CH_{2COD}), 32.1 (–CH_3), 30.2 (CH_{2COD}), 28.8 (–CH_3), 28.6 (CH_{2COD}). ^{19}F NMR (376 MHz, $CDCl_3$) δ −112.76 (CF_{Ar}). HR-MS electrospray ($DART^+$): calc. mass: 603.17473 *m*/*z* for $^{12}C_{23}{}^1H_{27}{}^{19}F_1{}^{193}Ir_1{}^{14}N_4{}^{16}O_2$ $[M - {}^{35}Cl_1]^+$. Found: 603.17643 *m*/*z*. Mass difference: 1.71 ppm. Elem. anal. calcd for $C_{23}H_{27}ClFIrN_4O_2$: C, 43.29; H, 4.26; N, 8.78. Found: C, 43.33; H, 4.16; N, 8.99. Melting point: 203.0–205.1 °C. HPLC relative purity: 96.07%.

*Complex (**3c**).* For the synthesis of (**3c**) was used $[IrClCOD]_2$ (168 mg, 0.25 mmol), potassium *tert*-butoxide (58 mg, 0.51 mmol) and (**2c**) (195 mg, 0.50 mmol). Yield: 182 mg (56.9%). ^{1}H NMR (500 MHz, $CDCl_3$) δ 7.57–7.54 (m, 2H, CH_{Ar}), 7.01–6.97 (m, 2H, CH_{Ar}), 6.14 (d, $^2J_{H-H}$ = 14.3 Hz, 1H, –CH_2–), 5.80 (d, $^2J_{H-H}$ = 14.3 Hz, 1H, –CH_2–), 4.87–4.84 (m, 1H, CH_{COD}), 4.74–4.70 (m, 1H, CH_{COD}), 4.49 (s, 3H, –CH_3), 3.78 (s, 3H, –CH_3), 3.31 (s, 3H, –CH_3), 2.93–2.90 (m, 1H, CH_{COD}), 2.64–2.60 (m, 1H, CH_{COD}), 2.33–2.15 (m, 3H, CH_{2COD}), 2.08–2.00 (m, 1H, CH_{2COD}), 1.94–1.88 (m, 1H, CH_{2COD}), 1.78–1.68 (m, 2H, CH_{2COD}), 1.54–1.47 (m, 1H, CH_{2COD}). $^{13}C\{^1H\}$ NMR (126 MHz, $CDCl_3$) δ 188.4 (C_{NHC-Ir}), 162.54 (d, $^1J_{C-F}$ = 246.3 Hz, CF_{Ar}), 152.6 (C═O), 150.7 (C═O), 140.9 ($C_{theophy}$), 132.2–132.1 (C_{Ar}), 130.2–130.1 (CH_{Ar}), 115.5–115.3 (CH_{Ar}), 109.5 ($C_{theophy}$), 88.7 (CH_{COD}), 87.9 (CH_{COD}), 53.7 (CH_{COD}), 52.9 (CH_{COD}), 52.6 (–CH_2–), 39.1 (–CH_3), 34.5 (CH_{2COD}), 32.6 (CH_{2COD}), 32.1 (–CH_3), 30.3 (CH_{2COD}), 28.7 (CH_{2COD}), 28.6 (–CH_3). ^{19}F NMR (376 MHz, $CDCl_3$) δ −114.40 (CF_{Ar}). HR-MS electrospray ($DART^+$): calc. mass: 638.14358 *m*/*z* for $^{12}C_{23}{}^1H_{27}{}^{35}Cl_1{}^{19}F_1{}^{193}Ir_1{}^{14}N_4{}^{16}O_2$ $[M]^+$. Found: 638.14662 *m*/*z*. Mass difference: 4.76 ppm. Elem. anal. calcd for $C_{23}H_{27}ClFIrN_4O_2$: C, 43.29; H, 4.26; N, 8.78. Found: C, 43.69; H, 4.32; N, 8.95. Melting point: 216.0–218.5 °C. HPLC relative purity: 95.91%.

*Complex (**3d**).* For the synthesis of (**3d**) was used $[IrClCOD]_2$ (168 mg, 0.25 mmol), potassium *tert*-butoxide (58 mg, 0.51 mmol) and (**2d**) (231 mg, 0.50 mmol). Yield: 160 mg (45.2%). ^{1}H NMR (500 MHz, $CDCl_3$) δ 6.43 (d, $^2J_{H-H}$ = 15.5 Hz, 1H, –CH_2–), 5.73 (d, $^2J_{H-H}$ = 15.5 Hz, 1H, –CH_2–), 4.72–4.68 (m, 1H, CH_{COD}), 4.66–4.62 (m, 1H, CH_{COD}), 4.48 (s, 3H, –CH_3), 3.81 (s, 3H, –CH_3), 3.38 (s, 3H, –CH_3), 2.97–2.94 (m, 1H, CH_{COD}), 2.71–2.67 (m, 1H, CH_{COD}), 2.40–2.24 (m, 2H, CH_{2COD}), 2.17–2.07 (m, 2H, CH_{2COD}), 1.96–1.91 (m, 1H, CH_{2COD}), 1.83–1.78 (m, 1H, CH_{2COD}), 1.67–1.60 (m, 1H, CH_{2COD}), 1.52–1.46 (m, 1H, CH_{2COD}). $^{13}C\{^1H\}$ NMR (126 MHz, $CDCl_3$) δ 190.6 (C_{NHC-Ir}), 153.1 (C═O), 150.6 (C═O), 146.6 (CF_{Ar}), 144.6 (CF_{Ar}), 142.3 (CF_{Ar}), 140.2 ($C_{theophy}$), 138.9 (CF_{Ar}), 137.0 (CF_{Ar}), 110.8 (C_{Ar}), 110.2 ($C_{theophy}$), 89.9 (CH_{COD}), 88.8 (CH_{COD}), 54.1 (CH_{COD}), 51.2 (CH_{COD}), 41.1 (–CH_2–), 39.5 (–CH_3), 35.0 (CH_{2COD}), 32.3 (CH_{2COD}), 32.1 (–CH_3), 30.0 (CH_{2COD}), 28.8 (–CH_3), 28.0 (CH_{2COD}). ^{19}F NMR (376 MHz, $CDCl_3$) δ −141.9 (CF_{Ar}), −154.3 (CF_{Ar}), −162.2. (CF_{Ar}). HR-MS electrospray ($DART^+$): calc. mass: 710.10589 *m*/*z* for $^{12}C_{23}{}^1H_{23}{}^{35}Cl_1{}^{19}F_5{}^{193}Ir_1{}^{14}N_4{}^{16}O_2$ $[M]^+$. Found: 710.10521 *m*/*z*. Mass difference: −0.95 ppm. Elem. anal. calcd for $C_{23}H_{23}ClF_5IrN_4O_2$: C, 38.90; H, 3.26; N, 7.89. Found: C, 38.88; H, 3.18; N, 8.15. Melting point: 178.2–179.5 °C. HPLC relative purity: 97.31%.

*Complex (**3e**).* For the synthesis of (**3e**) was used $[IrClCOD]_2$ (168 mg, 0.25 mmol), potassium *tert*-butoxide (58 mg, 0.51 mmol) and (**2e**) (204 mg, 0.50 mmol). Yield: 199 mg (60.6%). ^{1}H NMR (700 MHz, $CDCl_3$) δ 7.28–7.24 (m, 1H), 6.89–6.86 (m, 2H), 6.34 (d, $^2J_{H-H}$ = 15.6 Hz, 1H), 5.89 (d, $^2J_{H-H}$ = 15.6 Hz, 1H), 4.77–4.74 (m, 1H), 4.62–4.59 (m, 1H), 4.48 (s, 3H), 3.80 (s, 3H), 3.36 (s, 3H), 2.99–2.96 (m, 1H), 2.59–2.56 (m, 1H), 2.37–2.25 (m, 2H), 2.10–2.04 (m, 1H), 1.91–1.82 (m, 2H), 1.81–1.77 (m, 1H), 1.36–1.31 (m, 2H). $^{13}C\{^1H\}$ NMR (176 MHz, $CDCl_3$) δ 190.0 (C_{NHC-Ir}), 161.38 (dd, $^1J_{C-F}$ = 249.5, $^4J_{F-F}$ = 7.7 Hz, 2 × CF_{Ar}), 153.0 (C═O), 150.8 (C═O), 140.1 ($C_{theophy}$), 129.8–129.7 (CH_{Ar}), 113.5–113.3 (C_{Ar}), 111.9–111.7 (2 × CH_{Ar}), 110.7 ($C_{theophy}$), 89.3 (CH_{COD}), 87.6 (CH_{COD}), 53.9 (CH_{COD}), 51.3 (CH_{COD}), 42.5–42.4 (–CH_2–), 39.3 (–CH_3), 35.2 (CH_{2COD}), 32.1 (–CH_3), 32.0 (CH_{2COD}), 30.2 (CH_{2COD}), 28.8 (–CH_3), 27.9 (CH_{2COD}). ^{19}F NMR (282 MHz, $CDCl_3$) δ −113.74 (CF_{Ar}). HR-MS electrospray ($DART^+$): calc. mass: 656.13416 *m*/*z* for

$^{12}C_{23}{}^{1}H_{26}{}^{35}Cl_1{}^{19}F_2{}^{193}Ir_1{}^{14}N_4{}^{16}O_2$ $[M]^+$. Found: 656.13608 *m*/*z*. Mass difference: 2.93 ppm. Elem. anal. calcd for $C_{23}H_{26}ClF_2IrN_4O_2$: C, 42.10; H, 3.99; N, 8.54. Found: C, 42.41; H, 4.15; N, 8.95. Melting point: 188.3–191.1 °C. HPLC relative purity: 95.31%.

4.2.4. General procedure for the synthesis of Ir(I)–NHC complexes with CO (4a–e). In a vial, 100 mg of the corresponding NHC–Ir(I) complex (**3a–e**) was dissolved in DCM (5 mL) and the solution was cooled in an ice bath. Carbon monoxide was then bubbled through the mixture for 20 minutes. After this, all volatiles were removed under high vacuum. The resulting crude product was purified by washing with hexane, affording the desired compound.

*Complex (**4a**).* Yield: 88.1%. ^{1}H NMR (700 MHz, $CDCl_3$) δ 7.30–7.27 (m, 1H, CH_{Ar}), 7.17–7.15 (m, 1H, CH_{Ar}), 7.10–7.06 (m, 2H, CH_{Ar}), 6.03 (d, $^2J_{H-H}$ = 15.4 Hz, 1H, –CH_2–), 5.99 (d, $^2J_{H-H}$ = 15.4 Hz, 1H, –CH_2–), 4.38 (s, 3H, –CH_3), 3.84 (s, 3H, –CH_3), 3.34 (s, 3H, –CH_3). ^{13}C NMR (176 MHz, $CDCl_3$) δ 181.3 (C_{NHC-Ir}), 180.1 (Ir–CO), 167.0 (Ir–CO), 160.36 (d, $^1J_{C-F}$ = 248.0 Hz, CF_{Ar}), 152.7 (C═O), 150.7 (C═O), 140.5 ($C_{theophy}$), 130.1 (CH_{Ar}), 128.9 (CH_{Ar}), 124.3 (CH_{Ar}), 122.9 (C_{Ar}), 115.7 (CH_{Ar}), 109.8 ($C_{theophy}$), 48.1 (–CH_2–), 40.2 (–CH_3), 32.2 (–CH_3), 28.9 (–CH_3). MS (FAB^+): *m*/*z* 587 $[M + H]^+$. IR ($\tilde{\nu}$, cm^{-1}): 2924.03, 2061.57, 1977.25, 1710.12, 1664.98.

*Complex (**4b**).* Yield: 81.1%. ^{1}H NMR (700 MHz, $CDCl_3$) δ 7.34–7.26 (m, 2H, CH_{Ar}), 7.21–7.17 (m, 1H, CH_{Ar}), 7.02–6.95 (m, 1H, CH_{Ar}), 5.96 (d, $^2J_{H-H}$ = 14.7 Hz, 1H, –CH_2–), 5.87 (d, $^2J_{H-H}$ = 14.7 Hz, 1H, –CH_2–), 4.36 (s, 3H, –CH_3), 3.83 (s, 3H, –CH_3), 3.36 (s, 3H, –CH_3). ^{13}C NMR (176 MHz, $CDCl_3$) δ 180.5 (C_{NHC-Ir}), 180.0 (Ir–CO), 167.1 (Ir–CO), 162.93 (d, $^1J_{C-F}$ = 246.7 Hz, CF_{Ar}), 152.8 (C═O), 150.6 (C═O), 140.8 ($C_{theophy}$), 137.6 (C_{Ar}), 130.4–130.3 (CH_{Ar}), 124.0 (CH_{Ar}), 115.5–115.4 (CH_{Ar}), 115.2–115.1 (CH_{Ar}), 109.5 ($C_{theophy}$), 53.0 (–CH_2–), 40.1 (–CH_3), 32.2 (–CH_3), 28.9 (–CH_3). MS (FAB^+): *m*/*z* 587 $[M + H]^+$. IR ($\tilde{\nu}$, cm^{-1}): 2923.82, 2854.18, 2063.39, 1977.89, 1709.12, 1664.01.

*Complex (**4c**).* Yield: 85.9%. ^{1}H NMR (700 MHz, $CDCl_3$) δ 7.62–7.57 (m, 2H, CH_{Ar}), 7.04–6.96 (m, 2H, CH_{Ar}), 5.94 (d, $^2J_{H-H}$ = 14.4 Hz, 1H, –CH_2–), 5.84 (d, $^2J_{H-H}$ = 14.3 Hz, 1H, –CH_2–), 4.35 (s, 3H, –CH_3), 3.81 (s, 3H, –CH_3), 3.37 (s, 3H, –CH_3). ^{13}C NMR (176 MHz, $CDCl_3$) δ 180.2 (C_{NHC-Ir}), 180.0 (Ir–CO), 167.2 (Ir–CO), 162.86 (d, $^1J_{C-F}$ = 247.4 Hz, CF_{Ar}), 152.9 (C═O), 150.6 (C═O), 140.8 ($C_{theophy}$), 130.6 (CH_{Ar}), 126.1 (C_{Ar}), 115.7–115.6 (CH_{Ar}), 109.5 ($C_{theophy}$), 52.9 (–CH_2–), 40.1 (–CH_3), 32.2 (–CH_3), 28.9 (–CH_3). MS (FAB^+): *m*/*z* 587 $[M + H]^+$. IR ($\tilde{\nu}$, cm^{-1}): 2954.35, 2925.04, 2063.28, 1977.61, 1708.78, 1663.55, 1603.54.

*Complex (**4d**).* Yield: 84.9%. ^{1}H NMR (700 MHz, $CDCl_3$) δ 6.27 (d, $^2J_{H-H}$ = 15.6 Hz, 1H, –CH_2–), 5.83 (d, $^2J_{H-H}$ = 15.6 Hz, 1H, –CH_2–), 4.36 (s, 3H, –CH_3), 3.84 (s, 3H, –CH_3), 3.39 (s, 3H, –CH_3). ^{13}C NMR (176 MHz, $CDCl_3$) δ 182.4 (C_{NHC-Ir}), 179.8 (Ir–CO), 167.0 (Ir–CO), 153.1 (C═O), 150.5 (C═O), 146.2 (CF_{Ar}), 144.8 (CF_{Ar}), 142.5 (CF_{Ar}), 141.0 (CF_{Ar}), 140.2 ($C_{theophy}$), 138.7 (CF_{Ar}), 137.2 (CF_{Ar}), 110.0 ($C_{theophy}$), 109.8–109.6 (C_{Ar}), 42.9 (–CH_2–), 40.4 (–CH_3), 32.2 (–CH_3), 29.0 (–CH_3). MS (FAB^+): *m*/*z* 623 $[M - Cl]^+$. IR ($\tilde{\nu}$, cm^{-1}): 2932.72, 2854.10, 2068.02, 1976.05, 1711.93, 1661.93, 1711.93, 1661.93.

*Complex (**4e**).* Yield: 87.6%. ^{1}H NMR (700 MHz, $CDCl_3$) δ 7.33–7.26 (m, 1H, CH_{Ar}), 6.93–6.86 (m, 2H, CH_{Ar}), 6.13 (d, $^2J_{H-H}$ = 15.4 Hz, 1H, –CH_2–), 5.93 (d, $^2J_{H-H}$ = 15.5 Hz, 1H, –CH_2–), 4.35 (s, 3H, –CH_3), 3.83 (s, 3H, –CH_3), 3.38 (s, 3H, –CH_3). ^{13}C NMR (176 MHz, $CDCl_3$) δ 182.2 (C_{NHC-Ir}), 180.2 (Ir–CO), 166.9 (Ir–CO), 161.35 (dd, $^1J_{C-F}$ = 250.1 Hz, $^3J_{C-F}$ = 7.4 Hz, CF_{Ar}), 153.0 (C═O), 150.6 (C═O), 140.1 ($C_{theophy}$), 130.5–130.4 (CH_{Ar}), 112.2–112.0 (C_{Ar}), 111.9–111.8 (CH_{Ar}), 110.3 ($C_{theophy}$), 43.3 (–CH_2–), 40.3 (–CH_3), 32.2 (–CH_3), 28.9 (–CH_3). MS (FAB^+): *m*/*z* 576 $[M - CO]^+$. IR ($\tilde{\nu}$, cm^{-1}): 2962.75, 2924.06, 2059.49, 1973.34, 1709.78, 1661.48.

4.3. Cytotoxic evaluation

4.3.1. Cell lines culture and culture medium. All free ligands and iridium complexes were evaluated *in vitro* against a panel of human cancer cell lines: HCT-15 (colorectal adenocarcinoma), MCF-7 (mammary adenocarcinoma), K-562 (chronic myelogenous leukemia), U-251 (glioblastoma), PC-3 (prostatic adenocarcinoma), and SKLU-1 (lung adenocarcinoma), as well as COS-7 (healthy African green monkey kidney cells). The cell lines were obtained from the National Cancer Institute (USA). Cytotoxic activity against the tumor cells was assessed using the sulforhodamine B (SRB) protein-binding dye in a microculture assay to measure cell proliferation, following protocols established by the NCI.[1] Cells were cultured in RPMI-1640 medium supplemented with 10% fetal bovine serum, 2 mM L-glutamine, 10 000 units per mL penicillin G sodium, 10 000 μg mL^{-1} streptomycin sulfate, 25 μg mL^{-1} amphotericin B (Gibco), and 1% non-essential amino acids (Gibco). Cultures were maintained at 37 °C in a humidified atmosphere containing 5% CO_2. The viability of the cells used in the assays exceeded 95%, as determined by the trypan blue exclusion method.

4.3.2. Cytotoxic assay. Cytotoxicity after treatment of tumor and normal cells with the test compounds was determined using the sulforhodamine B (SRB) protein-binding dye in a microculture assay to measure cell growth. Cells were detached from tissue culture flasks using trypsin and then diluted in fresh medium. Aliquots of 100 μL of the resulting cell suspension, containing 5000–10 000 cells per well, were seeded into 96-well microtiter plates (Costar) and incubated at 37 °C for 24 h in a humidified atmosphere with 5% CO_2. Subsequently, 100 μL of the test compound solution—prepared by diluting stock solutions—were added to each well. The cultures were exposed to the compound at a concentration of 50 μM for 48 h. After the incubation period, cells were fixed to the plastic substrate by adding 50 μL of cold 50% aqueous trichloroacetic acid. The plates were incubated at 4 °C for 1 h, washed with tap water, and air-dried. The fixed cells were then stained with 0.4% SRB solution. Unbound dye was removed by washing with 1% aqueous acetic acid. Afterward, the plates were air-dried, and the protein-bound dye was solubilized by adding 100 μL of 10 mM unbuffered Tris base. The plates were shaken for

10 min, and absorbance was measured at 515 nm using an ELISA plate reader (Bio-Tek Instruments).

Conflicts of interest

The authors declare no conflicts of interest.

Data availability

The data supporting this article has been included as part of the ESI.†

Acknowledgements

We would like to thank Chem. Eng. Luis Velasco Ibarra, Dr Francisco Javier Pérez Flores, Q. Eréndira García Ríos, MSc Lucia del Carmen Márquez Alonso, MSc Lucero Ríos Ruiz, MSc Alejandra Núñez Pineda (CCIQS), Q. María de la Paz Orta Pérez, Q. Roció Patiño-Maya and PhD Nuria Esturau Escofet for technical assistance. Arturo S. would like to thank CONAHCyT (No. CVU: 848539) and Fundación Telmex-Telcel (Folio: 212009996) for the PhD scholarship granted. The financial support of this research by UNAM-DGAPA-PAPIIT IN223323 is gratefully acknowledged.

References

1 F. Bray, M. Laversanne, H. Sung, J. Ferlay, R. L. Siegel, I. Soerjomataram and A. Jemal, *Ca-Cancer J. Clin.*, 2024, **74**, 229–263.
2 A. Casini and A. Pöthig, *ACS Cent. Sci.*, 2024, **10**, 242–250.
3 Q. Peña, A. Wang, O. Zaremba, Y. Shi, H. W. Scheeren, J. M. Metselaar, F. Kiessling, R. M. Pallares, S. Wuttke and T. Lammers, *Chem. Soc. Rev.*, 2022, **51**, 2544–2582.
4 K. J. Franz and N. Metzler-Nolte, *Chem. Rev.*, 2019, **119**, 727–729.
5 M. M. González-Ballesteros, C. Mejía and L. Ruiz-Azuara, *FEBS Open Bio*, 2022, **12**, 880–899.
6 L. H. Delgado-Rangel, V. Reyes-Márquez, M. E. Moreno-Narváez, A. Aragón-Muriel, J. R. Parra-Unda, J. A. Cruz-Navarro, M. A. Martínez-Torres, H. Valdés and D. Morales-Morales, *New J. Chem.*, 2025, **49**, 3442–3455.
7 A. Sánchez-Mora, E. Briñez, A. Pico, L. González-Sebastián, J. Antonio Cruz-Navarrro, A. Arenaza-Corona, N. Puentes-Díaz, J. Alí-Torres, V. Reyes-Márquez and D. Morales-Morales, *Chem. Biodiversity*, 2024, **21**, e202400995.
8 A. Amaya-Flórez, J. S. Serrano-García, J. Ruiz-Galindo, A. Arenaza-Corona, J. A. Cruz-Navarro, A. L. Orjuela, J. Alí-Torres, M. Flores-Alamo, P. Cano-Sanchez, V. Reyes-Márquez and D. Morales-Morales, *Front. Chem.*, 2024, **12**, 1483999.
9 A. Arenaza-Corona, P. Sánchez-Portillo, L. González-Sebastián, A. Sánchez-Mora, B. Monroy-Torres, T. Ramírez-Apan, N. Puentes-Díaz, J. Alí-Torres, V. Barba, V. Reyes-Marquez and D. Morales-Morales, *Chem. Biodiversity*, 2025, **22**, e202402083.
10 S. A. Patil, A. P. Hoagland, S. A. Patil and A. Bugarin, *Future Med. Chem.*, 2020, **12**, 2239–2275.
11 Y.-F. Zhang, Y.-K. Yin, H. Zhang and Y.-F. Han, *Coord. Chem. Rev.*, 2024, **514**, 215941.
12 K. O. Marichev, S. A. Patil, S. A. Patil, H. M. Heras Martinez and A. Bugarin, *Expert Opin. Ther. Pat.*, 2022, **32**, 47–61.
13 H. Valdés, D. Canseco-González, J. M. Germán-Acacio and D. Morales-Morales, *J. Organomet. Chem.*, 2018, **867**, 51–54.
14 M. O. Dar, R. H. Mir, R. Mohiuddin, M. H. Masoodi and F. A. Sofi, *J. Inorg. Biochem.*, 2023, **246**, 112290.
15 H. A. Mohamed, B. R. M. Lake, T. Laing, R. M. Phillips and C. E. Willans, *Dalton Trans.*, 2015, **44**, 7563–7569.
16 T. Scattolin, I. Caligiuri, L. Canovese, N. Demitri, R. Gambari, I. Lampronti, F. Rizzolio, C. Santo and F. Visentin, *Dalton Trans.*, 2018, **47**, 13616–13630.
17 Y. Gothe, T. Marzo, L. Messori and N. Metzler-Nolte, *Chem. Commun.*, 2015, **51**, 3151–3153.
18 Y. Gothe, I. Romero-Canelón, T. Marzo, P. J. Sadler, L. Messori and N. Metzler-Nolte, *Eur. J. Inorg. Chem.*, 2018, 2461–2470.
19 Y. Gothe, T. Marzo, L. Messori and N. Metzler-Nolte, *Chem. – Eur. J.*, 2016, **22**, 12487–12494.
20 M. O. Karataş, G. Şekerci, S. Tekin, S. Sandal and H. Küçükbay, *J. Coord. Chem.*, 2023, **76**, 1507–1517.
21 M. Olgun Karataş, T. Keskin, N. Özdemir, H. Küçükbay, S. Tekin, A. Mansur, S. Günal and S. Sandal, *Inorg. Chem. Commun.*, 2022, **146**, 110080.
22 A. Sánchez-Mora, H. Valdés, M. T. Ramírez-Apan, A. Nieto-Camacho, S. Hernández-Ortega, D. Canseco-González and D. Morales-Morales, *Inorg. Chim. Acta*, 2019, **496**, 119061.
23 I. Eslava-Gonzalez, H. Valdés, M. Teresa Ramírez-Apan, S. Hernandez-Ortega, M. Rosario Zermeño-Ortega, A. Avila-Sorrosa and D. Morales-Morales, *Inorg. Chim. Acta*, 2020, **507**, 119588.
24 E. Rufino-Felipe, R. Colorado-Peralta, V. Reyes-Márquez, H. Valdés and D. Morales-Morales, *Anticancer Agents Med. Chem.*, 2020, **21**, 938–948.
25 J. C. Páez-Franco, M. R. Zermeño-Ortega, C. M. de la O-Contreras, D. Canseco-González, J. R. Parra-Unda, A. Avila-Sorrosa, R. G. Enríquez, J. M. Germán-Acacio and D. Morales-Morales, *Pharmaceutics*, 2022, **14**, 402.
26 Z. Li, Q. Zhang, H. Liu, G. Wang and J. Liu, *Dyes Pigm.*, 2019, **163**, 647–655.
27 A. Łukaszewicz-Hussain, J. Moniuszko-Jakoniuk and J. Rogalska, *Pol. J. Environ. Stud.*, 2007, **16**, 233–236.
28 I. M. Daubit and N. Metzler-Nolte, *Dalton Trans.*, 2019, **48**, 13662–13673.
29 N. D. Donahue, H. Acar and S. Wilhelm, *Adv. Drug Delivery Rev.*, 2019, **143**, 68–96.
30 A. Andrés, M. Rosés, C. Ràfols, E. Bosch, S. Espinosa, V. Segarra and J. M. Huerta, *Eur. J. Pharm. Sci.*, 2015, **76**, 181–191.